



Physical and chemical properties of binary mixtures of dibutylammonium-based ionic liquids and water

Fábio Costa¹ · Fernanda S. Paixão¹ · Alexandre S. Zimmermann¹ · Ana Cristina Morais da Silva² · Silvana Mattedi¹

Received: 13 January 2021 / Revised: 29 August 2021 / Accepted: 10 October 2021 / Published online: 15 November 2021
© Associação Brasileira de Engenharia Química 2021

Abstract

Ionic liquids are used in different processes owing to their low vapor pressure, large viscosity range, chemical and thermal stability, and superior conductance even without water. These features make them flexible and tunable, indicating their possible use as substitutes for commonly used compounds in many processes. The objective of this study was to evaluate the properties of aqueous binary solutions for three different ionic liquids (ILs): dibutylammonium acetate, dibutylammonium propanoate, and dibutylammonium butanoate. The measured properties were density, speed of sound, and conductivity, and their isentropic compressibility and thermal expansion coefficient were calculated based on these properties. The temperature range used for measurements was 293.15–323.15 K. Mathematical models were used for each ionic liquid + water mixture to fit the density and speed of sound data. The increase in the alkyl chain leads to a tendency to decrease the values of density, speed of sound, and conductivity of the solutions. However, decreasing the dilution in water, the density, the conductivity and the speed of sound initially increase and then decrease, exhibiting a maximum in the initial water concentration range which indicates the formation of aggregates. Critical micellar concentrations at 298 K were determined through conductivity data. Enhancing the temperature leads to a decrease on density and sound velocity.

Keywords Ionic liquids · Density · Speed of sound · Conductivity · Critical micellar concentration · Properties

Introduction

The need for new, more environmentally friendly solvents to replace or reduce the use of popular solvents currently employed in the industry and academia is increasing. Ionic liquids (ILs) have gained industrial and academic interest for their potential use as ecological solvents to replace traditional volatile solvents. Ionic liquids, according to Rogers and Seddon (2003), are chemical compounds that are liquids at temperatures below or around 373.15 K and are entirely formed by ions. Protic ionic liquids (PILs) are salts formed by a neutralization reaction described by the Brønsted–Lowry acid–base model, whereas aprotic ionic liquids (AILs) are salts that are formed following the Lewis model (Yoshizawa et al. 2003; MacFarlane and Seddon 2007). The

main difference between a PIL and an AIL is the fact that the PIL has protic hydrogen, that is, mobile hydrogen, whereas AILs do not, because the latter's pathway acid is a Lewis acid (Bittencourt et al. 2017).

ILs present several advantages, including low vapor pressure, as they are ionic structures with a high degree of cohesion (Alvarez et al. 2013). They are also highly tunable, and can be designed for different purposes, for example, used in wastewater treatment (Kong et al. 2019), as conductive ink (Darabi and Shabani-Nooshabadi 2021), as a component of emulsifying systems for oil enhanced recovery (Jabbari et al. 2019), and for electrochemical devices such as in the synthesis of SARS-CoV-2 detection electrodes (Fabiani et al. 2021), among others. They have excellent electrical conductance, and are widely used in electrochemical systems such as fuel cells and anhydrous electrolytes. They are thermally stable and can be used over a wide temperature range (Khan et al. 2018; Santos et al. 2018).

The viability of PIL synthesis allows for a wide variety of cation and anion combinations because of its simplicity (Xu et al. 2012; Greaves et al. 2015). Each combination yields different physical and chemical properties; therefore,

✉ Silvana Mattedi
silvana@ufba.br

¹ Chemical Engineering Graduate Program, Federal University of Bahia, Salvador, Brazil

² Materials Science and Technology Department, Federal University of Bahia, Salvador, Brazil

knowledge of these properties is necessary for the development of new applications. Protic ILs have been applied in the development of conductive membranes, ensuring that the membrane has a higher conductivity than its pure version, therefore reducing the need for polymer hydration and increasing membrane strength and conductivity (Li et al. 2019; Nair and Mohapatra 2019). Moreover, PILs based on ammonium and carboxylate anions as well as choline salts have been reported to be among the most biodegradable ILs and could feasibly be used as solvent additives in biological media (Arunkumar et al. 2020). However, studies carried out by Oliveira et al. (2016) showed that for a series of ILs based on *N*-methyl-2-hydroxyethylammonium cations combined with carboxylate anions ranging from acetate to pentanoate, a longer alkyl chain increases the toxicity of the IL.

In this study, the measured properties were the density, speed of sound, and conductivity. The speed of sound is an important physicochemical property for the development of equations of state and is mathematically related to several thermodynamic properties, such as the isobaric or isovolumetric heat capacity, Joule–Thomson coefficient, isentropic compressibility, and apparent isentropic compressibility (Alvarez et al. 2011; Musale et al. 2018).

Knowledge of the density of ILs is important for several chemical processes and for studies based on chemical theories that can be used to create experimental databases, which provide IL properties under different conditions. Because ILs are solvents that can be implemented in various chemical processes, knowing their properties, especially their density, is critical. From these density data, it is possible to calculate the thermal expansion coefficient (Pinto et al. 2015). Knowledge of the density and derived thermodynamic properties can provide useful insight into interactions at the molecular level, such as evaluating the solvent's isothermal compressibility. However, its measurement is often not sufficiently accurate or is excessively time-consuming. The utilization of isentropic compressibility is a viable alternative, as it can be obtained more accurately through a simple calculation using the speed of sound and density data (Malik et al. 2021, Musale et al. 2018). For example, Shekaari et al. (2021) studied the behavior of the IL aqueous mixtures: choline alaninate, choline glycinate, and choline valinate, in order to assess the interactions between their functional groups and water, and it was shown that the length of the anion chain has a direct effect on the interaction between the IL and the solvent. Shekaari et al. (2008) used isentropic compressibility as an indication of clathrate formation in mixtures of water and 1-hexyl-3-methyl-imidazolium bromide.

The thermal expansion coefficient can also be used to understand the behavior of substances and mixtures at a microscopic level and plays an important theoretical role. As it is a second cross-derivative of the thermodynamic potential, it can be directly related to the equations of state; thus,

it is an important tool for the evaluation of existing equations of state and design of new ones. Basouli et al. (2021) and Song et al. (2021) studied the molecular dynamics and properties of ILs based on the thermal expansion coefficient to understand the behavior of conductivity and ionic interactions within ILs.

Conductivity studies are important because of the great potential of ILs in electrochemical applications, such as in energy storage devices (Lu et al. 2002; Sakaebe and Matsumoto 2003; Buzzeo et al. 2004; Armand et al. 2009; Borgel et al. 2009; Balducci et al. 2011; Shiddiky and Torriero 2011; Kar et al. 2013; Eftekhari et al. 2016; Mert et al. 2018; Rosales et al. 2019). Electrochemical impedance spectroscopy (EIS) is one of the most complete techniques available for the analysis, characterization, and development of electrochemical and electro-physical circuits (Cervera et al. 2014), and is favored over a simple conductivity analysis to obtain more accurate results for the conductivity of ionic liquid solutions.

In this study, three PILs were used based on the reaction of dibutylamine with linear carboxylic acids with two, three, and four carbons to form dibutylammonium acetate [DBA][Ac], dibutylammonium propanoate [DBA][Pr], and dibutylammonium butanoate [DBA][Bu]. This selection of anionic sources was chosen in order to analyze how the variation of the acidic carbon chain, as well as different concentrations of ionic liquid in water, influences the properties discussed above. At the completion of this article, no data were found in the literature that matched the data obtained by the analyses carried out in this study.

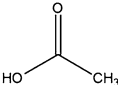
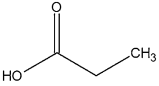
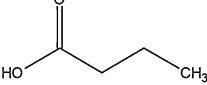
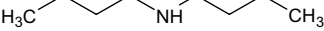
Methodology

Synthesis

All reagents used for the synthesis of the three ionic liquids were supplied by Sigma-Aldrich with a purity greater than 0.999 g/g (Table 1).

To carry out the synthesis, a magnetic stirrer, a three-neck round-bottom flask, and a dropping funnel were used. The reagents were weighed with respect to the 1:1 molar stoichiometry, and the base was placed in the flask and the acid in the funnel. Dripping of the acid on the base took place under constant magnetic stirring. The reaction was conducted in a nitrogen gas atmosphere to minimize moisture. After adding the acid, stirring continued for another 20 min to ensure homogeneity of the PIL (Alvarez et al. 2013). The liquids were kept in closed amber flasks inside desiccators to minimize photochemical reactions and absorption of atmospheric moisture, respectively. Three PILs were synthesized for evaluation: dibutylammonium acetate [DBA]

Table 1 Reagents used in the synthesis

Reagent	CAS	Structure	Purity ^a	Supplier
Acetic acid	64-19-7		≥ 0.999	Sigma Aldrich
Propanoic acid	79-09-4		≥ 0.999	Sigma Aldrich
Butanoic acid	107-92-6		≥ 0.999	Sigma Aldrich
Dibutylamine	111-92-2		≥ 0.999	Sigma Aldrich

^aThese materials were used as-received; purity was based on gas chromatography data provided by the supplier.

[Ac], dibutylammonium propanoate [DBA][Pr], and dibutylammonium butanoate [DBA][Bu].

NMR

The IL samples were diluted in deuterated chloroform (CDCl₃) (approximately 400 μL), the solution was then transferred to 5 mm nuclear magnetic resonance (NMR) tubes, and the ¹H and ¹³C spectra were obtained at 293 K using a Varian 500 spectrometer (500 MHz for ¹H, Agilent Technologies, Ltd., Santa Clara, CA) and tetramethylsilane (TMS) was used as the zero standard. All spectra were analyzed using the MestReNova software package. Purity was determined from the deviation of the values of the integrals of the ¹H spectra.

Binary mixtures of ILs with water added

For the following analysis, samples of aqueous gravimetric solutions were obtained. The solutions were prepared using 20 ml vials, over the entire range of composition: from approximately 0.1–0.9 g/g. The IL and water components were weighed using an analytical balance (Shimadzu model AX200). The balance accuracy was estimated to be ±0.0001 g.

To improve the precision in the preparation of the solutions, the initial water content of the ILs, determined by Karl Fischer analysis (measured with a Mettler Toledo Karl-Fischer V20 volumetric titrator), was considered in the mass balance equation.

To guarantee the homogeneity of the concentrations of the solutions to be used to measure the physical–chemical properties of the IL, a unique solution was prepared for each of the ILs ([DBA][Ac], [DBA][Pr], and [DBA][Bu]). Using these solutions, aliquots were removed to determine the IL properties (Alcantara et al. 2018).

Density and speed of sound

The density and speed of sound were measured simultaneously, in duplicate, using an Anton Paar densimeter (Model DSA 5000). The equipment has two cells: one with an oscillating U-tube to measure the density and one that employs a pulse-echo to measure the speed of sound. Both allow for temperature control using internal Peltier elements with an accuracy of ±0.01 K. The tests were performed by ramping the temperature from 293.15 K to 323.15 K in 5 K increments. Measurement uncertainties were calculated. All experiments were performed under atmospheric pressure.

The density and speed of sound were fitted using Eq. (1),

$$Z = \sum_{i=0}^p \left(\sum_{j=0}^q B_{ij} T^j \right) w_2^i \quad (1)$$

where Z represents either the density or speed of sound of the mixture, w_2^i is the mass fraction of the solvent, p and q are the polynomial degrees, and B_{ij} are fitting parameters.

The absolute average relative deviation percentage (%AARD) and the coefficient of determination (R^2) for each correlation were calculated according to Eqs. (2) and (3), respectively, to evaluate the quality of the fit.

$$\%AARD = \frac{1}{N} \sum_{i=1}^N \left| \frac{y_i - t_i}{t_i} \right| \cdot 100 \quad (2)$$

$$R^2 = 1 - \frac{\sum_{i=1}^N (t_i - y_i)^2}{\sum_{i=1}^N (\bar{t}_i - y_i)^2} \quad (3)$$

Here, t is the experimental value, y is the correlated value, N is the number of samples, and the bar over a variable refers to its average value.

From the experimental results of the density and speed of sound measured from the ionic liquid mixtures, it was possible to calculate the thermal expansion coefficient (α) and isentropic compressibility (β_s). Equations (4) and (5) define α and β_s , respectively.

$$\alpha = -\frac{1}{\rho} \cdot \frac{\partial \rho}{\partial T} \quad (4)$$

$$\beta_s = \frac{1}{\nu^2 \cdot \rho} \quad (5)$$

ρ is the PIL density in g/cm^3 , ν is the speed of sound in m/s , and T is the temperature in K (Alvarez et al. 2011; Musale et al. 2018).

Conductivity

The electrochemical impedance measurements were carried out in a potentiostat/galvanostat equipped with an electrochemical impedance module unit ((FRA), model PGSTAT302 METROHM AUTOLAB). The data were analyzed using the Metrohm NOVA version 1.11 software package.

Duplicate measurements were taken at a temperature of 298.15 K, and the parameters used for the measurements were a simple sine wave with an amplitude of 0.01 V, scanning frequency of 100 kHz to 0.1 Hz, and potential of 1 V at 20 points per decade. All experiments were performed under atmospheric pressure.

From the impedance measurements obtained, the conductivity of the PIL solutions can be calculated using Eq. (9):

$$K = \frac{1}{R} \times k \quad (6)$$

where $k = L/A$, L is the distance between the electrodes, and A is the area of the electrodes. The electrode constant is $k = 1.04 \text{ cm}^{-1}$. R is the polarization resistance, which refers to the first positive point in the pair (x, y) in the Nyquist diagrams obtained, whose real and imaginary resistances are both positive (Rosales et al. 2019; Nascimento et al. 2020).

From statistical treatment of the data, the final Nyquist diagram was obtained from the mean values for the imaginary and real resistance, respectively, represented by the coordinate pair (Y, X).

Critical micellar concentration (CMC)

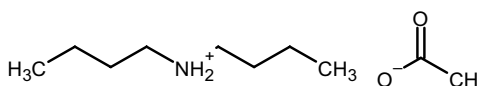
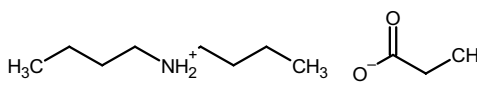
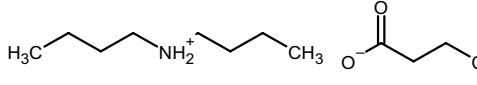
CMC was determined fitting a third-degree polynomial curve to conductivity data as a function of the IL fraction in the solution and subsequently differentiating it in terms of the fraction to find the maximum point in the curve. The curves fitted had a correlation coefficient (R^2) over 0.98 for all cases.

Results and discussion

The ^1H NMR and ^{13}C NMR spectra of the synthesized ILs ([DBA][Ac], [DBA][Pr], and [DBA][Bu]) are shown in the supplementary material in Figs. S1–S3. The chemical shifts and peak integrals are shown in the figures and correspond to the expected structures. None of the spectra exhibited any indication of contamination. The initial water content, purity, and the structure of the ILs are presented in Table 2.

Purity was determined from peak integration using the ^1H NMR spectra, reaching values of ca. 0.99 g/g. These values were of the same order as the ILs synthesized and published by Alcantara et al. (2018) and Nascimento et al. (2020), who used the same synthesis methodology.

Table 2 Ionic liquid structures, purity, and water content

Name	Structure	Purity* g/g	Water** g/g	Physical state ^a
Dibutylammonium Acetate [DBA][Ac]		0.9896	0.0023	Solid
Dibutylammonium Propanoate [DBA][Pr]		0.9894	0.0023	Solid
Dibutylammonium Butanoate [DBA][Bu]		0.9898	0.0021	Liquid

* $U_{\text{purity}} = \pm 0.0001$.

** $U_{\text{water- [Ac]}} = \pm 0.0003$; $u_{\text{water- [Pr]}} = \pm 0.0003$; $u_{\text{water- [Bu]}} = \pm 0.0005$.

^aObserved at $298 \pm 1 \text{ K}$ and $101.39 \pm 0.21 \text{ kPa}$.

As shown in Figs. S1–S3, the structure of each IL was confirmed by ^1H NMR spectroscopy. The dibutylammonium group presents a similar structure in all three ionic liquids, characterized by a methyl group and three methylene groups presenting typical chemical shifts for a butyl chain attached to nitrogen. The cation in [DBA][Ac] presented the signal $\delta 0.69$ (*t*, H-1, 6H) for methyl groups, whereas the signals for methylene groups were $\delta 1.14$ (*sex*, H-2, 4H), $\delta 1.46$ (*quin*, H-3, 4H), and $\delta 2.57$ (*t*, H-5, 4H). Similar results were obtained for the cation in [DBA][Pr]; the signals for the methyl groups were $\delta 0.34$ (*t*, H-1, 6H), and the methylene groups appeared at $\delta 0.8$ (*sex*, H-3, 4H), $\delta 1.12$ (*quin*, H-4, 4H), and $\delta 2.25$ (*t*, H-6, 4H). The cation in [DBA][Bu] presented a slightly different spectrum, as the methyl group in the butanoate anion overlapped with the methyl groups in the cation, thus modifying the peak multiplicity to a heptate, and the corresponding area of the peak is proportional to nine protons. In this case, the signals for the methyl groups were $\delta 0.47$ (*hep*, H-1, 9H), and the methylene groups appeared at $\delta 0.91$ (*sex*, H-2, 4H), $\delta 1.24$ (*quin*, H-4, 4H), $\delta 2.25$ (*quin*, H-6, 4H), and $\delta 9.3$ (*s*, H-7, 2H).

The acetate group presents the chemical shift of a typical methyl group connected to a carboxyl at $\delta 1.7$ (*s*, H-4, 3H) for acetate, whereas the methyl group for propanoate appeared at $\delta 0.5$ (*t*, H-2, 3H) and $\delta 1.6$ (*quin*, H-5, 2H). For butanoate, the methyl group overlapped with the methyl groups in the cation. The methylene signals were at $\delta 1.6$ (*quin*, H-2, 2H) for [Pr], while they were at $\delta 1.14$ (*sex*, H-2, 2H) and $\delta 1.66$ (*quin*, H-5, 2H) for [Bu]. The structure was also corroborated by ^{13}C NMR spectroscopy, with signals at ~ 810 to ~ 847 corresponding to carbons in the methyl and methylene groups. On the other hand, the carboxyl group peak occurred at $\delta 177$ – $\delta 180$ for the three anions.

Aqueous solutions of the three synthesized ILs were prepared to study the density, speed of sound, isentropic compressibility, thermal expansion coefficient, and conductivity of the ILs.

The density and speed of sound values were obtained from the analysis using the DSA 5000 densimeter, and Table 3 shows the relationship between the data obtained from the density and speed of sound analysis, as well as their respective uncertainties.

All solutions with concentrations of ~ 0.1 to ~ 0.9 g/g showed an increasing trend in the density value as more solvent was added. Because of the limitations of some equipment, it was decided not to work with the ionic structures in their pure form, as some analyses could not be performed owing to the solid state of pure [DBA][Ac] and [DBA][Pr], as indicated in Table 2. There was also a subtle decrease in the density value with an increase in temperature. These trends were expected because they have been commonly observed among other substances reported in the literature

(Alcantara et al. 2018; Song et al. 2021; Sarabando et al. 2019).

From the obtained results, it can be seen that the shorter the alkyl chain length, the greater the density value at a fixed temperature. For example, the density values measured for [DBA][Ac], [DBA][Pr], and [DBA][Bu], measured at an approximate concentration of 0.9 g/g and temperature of 323.15 K were 0.9158 g/cm 3 , 0.9004 g/cm 3 , and 0.8917 g/cm 3 , respectively. This behavior has been reported previously (Crespo et al. 2021; Pinkert et al. 2011; Keshapolla et al. 2019, Zailani et al. 2020). The density of ionic liquids that are more similar to the ionic liquids used in this work were reported by Zailani et al. (2020). They measured the pure ILs with the same cation of this work and carboxylate anions containing 5 to 7 carbons. They also measured densities of pure ILs with a smaller cation (diethylammonium) and the same anions. For ILs with both studied cations the behavior was like the one found in this work, decreasing the density as the alkyl chain length increases.

The studied IL density and speed of sound data reach a maximum point in the range of $w_{\text{IL}} = 0.2$ to 0.3 , as indicated in Fig. 1 for [DBA][Ac] and in Figs. S4 and S5 in the Supplementary Material for [DBA][Pr] and [DBA][Bu], respectively. These maximum points indicate a high level of interaction between water and the IL. The interactions between the IL cations and anions consist of a mixture of forces, including hydrogen bonds, electrostatic interactions, and dispersive forces. As the water concentration increases, the ions are increasingly solvated by the water molecules, promoting the appearance of new hydrogen bonds while simultaneously weakening the dispersive forces originating from the nonpolar areas of the ions (Alcantara et al. 2018). Musale et al. (2018) presented data for pure IL densities as well as the density and speed of sound of diluted aqueous mixtures of ILs based on diethylammonium cation [DEA] combined with carboxylate anions from formate to butyrate. Data show an increasing value in the diluted region (less than 0.1 g/g of IL) of the speed of sound when the IL content is enhanced. The same behavior is observed in this work leading to a maximum in the speed of sound in the diluted region. Increasing the anion chain length, the speed of sound increases, the same result was also observed in this work.

A maximum in the speed of sound in diluted aqueous solution as observed in this work could be explained by the presence of aggregates in the solution and micellar formation. This phenomenon was reported previously for different authors for ammonium carboxylate ionic liquids (Alvarez et al. 2011; Maximo et al. 2014; Yalsin et al. 2020).

A small deviation can be seen in the trend, which is more noticeable with respect to the speed of sound, as shown in Fig. 1b and Figs. S4(b) and S5(b) in the Supplementary Material. This deviation may be related to the formation of micelles in the range of approximately 0.1–0.4 g/g of the

Table 3 Properties of various [DBA][Ac], [DBA][Pr], and [DBA][Bu] mixtures combined with water, where w_1 is IL mass fraction, ρ is the density, $\sigma(\rho)$ is the standard deviation of density, ν is the speed of sound, $\sigma(\nu)$ is the standard deviation of the speed of sound, and T indicates the temperature and uncertainty (atmospheric pressure of 101.39 ± 0.21 kPa)

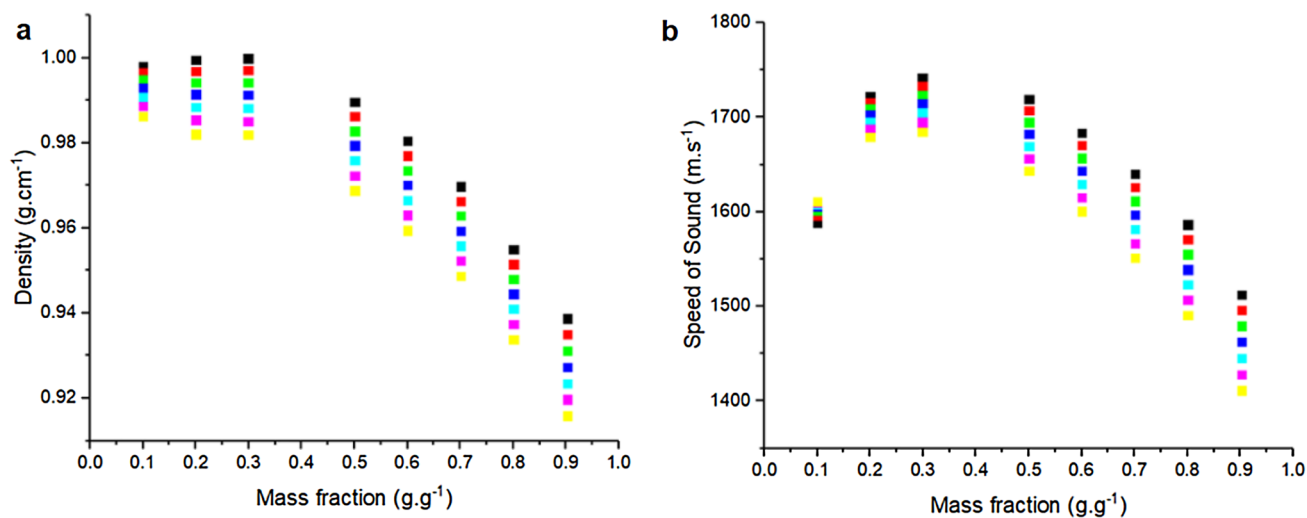
[DBA][Ac]				[DBA][Pr]				[DBA][Bu]			
w_1^a	ρ	$\sigma(\rho)$	ν	w_1^a	ρ	$\sigma(\rho)$	ν	w_1^a	ρ	$\sigma(\rho)$	ν
g/g	g/cm ³	g/cm ³	m/s	g/g	g/cm ³	g/cm ³	m/s	g/g	g/cm ³	g/cm ³	m/s
		\pm m/s				\pm m/s					
0.0997	0.9980	1.41×10^{-6}	1588.79	0.0998	0.9971	1.20×10^{-3}	1592.42	0.0909	0.9968	4.57×10^{-4}	1594.69
0.2000	0.9995	2.51×10^{-4}	1722.07	0.1990	0.9988	7.12×10^{-4}	1711.89	0.2002	0.9956	1.33×10^{-3}	1683.88
0.2990	0.9998	3.54×10^{-6}	1741.72	0.2995	0.9962	3.07×10^{-3}	1733.92	0.2996	0.9930	1.22×10^{-3}	1699.97
0.5003	0.9896	8.49×10^{-6}	1719.26	0.4012	0.9907	2.63×10^{-3}	1720.30	0.4002	0.9856	1.70×10^{-3}	1678.57
0.5997	0.9804	5.52×10^{-5}	1683.54	0.4981	0.9841	1.12×10^{-3}	1690.17	0.5987	0.9649	1.61×10^{-3}	1618.42
0.7012	0.9698	3.17×10^{-4}	1640.27	0.6003	0.9732	1.41×10^{-5}	1652.47	0.6996	0.9496	3.08×10^{-3}	1585.78
0.8010	0.9550	1.61×10^{-4}	1586.55	0.6995	0.9603	1.63×10^{-3}	1608.29	0.8966	0.9154	3.74×10^{-3}	1470.74
0.9019	0.9387	7.04×10^{-4}	1512.33	0.7985	0.9445	2.48×10^{-3}	1557.41				
				0.9006	0.9241	1.35×10^{-4}	1476.74				
0.0997	0.9965	1.41×10^{-6}	1595.58	0.0998	0.9954	1.18×10^{-3}	1598.82	0.0909	0.9947	7.59×10^{-4}	1600.59
0.2000	0.9969	3.56×10^{-4}	1715.80	0.1990	0.9963	8.12×10^{-4}	1705.81	0.2002	0.9922	8.15×10^{-4}	1679.50
0.2990	0.9971	1.27×10^{-5}	1732.73	0.2995	0.9923	1.99×10^{-3}	1724.30	0.2996	0.9898	1.23×10^{-3}	1690.80
0.5003	0.9863	1.41×10^{-6}	1707.33	0.4012	0.9871	2.74×10^{-3}	1709.69	0.4002	0.9820	1.69×10^{-3}	1668.85
0.5997	0.9770	5.66×10^{-5}	1670.34	0.4981	0.9805	9.62×10^{-4}	1678.22	0.5987	0.9608	1.21×10^{-3}	1605.37
0.7012	0.9663	3.66×10^{-4}	1626.00	0.6003	0.9696	2.52×10^{-4}	1638.70	0.6996	0.9450	2.46×10^{-3}	1571.18
0.8010	0.9515	1.46×10^{-4}	1570.85	0.6995	0.9567	1.45×10^{-3}	1593.33	0.8966	0.9113	3.22×10^{-3}	1453.39
0.9019	0.9350	4.26×10^{-4}	1495.93	0.7985	0.9404	1.83×10^{-3}	1541.04				
				0.9006	0.9176	1.81×10^{-3}	1460.21				
0.0997	0.9949	2.12×10^{-6}	1601.10	0.0998	0.9930	9.91×10^{-4}	1603.97	0.0909	0.9925	6.78×10^{-4}	1605.31
0.2000	0.9942	4.63×10^{-4}	1709.23	0.1990	0.9936	8.66×10^{-4}	1699.43	0.2002	0.9883	2.21×10^{-4}	1674.83
0.2990	0.9942	9.19×10^{-6}	1723.53	0.2995	0.9884	1.17×10^{-3}	1714.57	0.2996	0.9864	1.15×10^{-3}	1681.58
0.5003	0.9828	9.90×10^{-6}	1695.03	0.4012	0.9835	2.58×10^{-3}	1698.46	0.4002	0.9782	1.95×10^{-3}	1658.83
0.5997	0.9736	5.23×10^{-5}	1656.87	0.4981	0.9769	8.84×10^{-4}	1665.95	0.5987	0.9565	8.03×10^{-4}	1592.06
0.7012	0.9629	3.75×10^{-4}	1611.39	0.6003	0.9661	4.70×10^{-4}	1624.78	0.6996	0.9405	2.06×10^{-3}	1556.44
0.8010	0.9480	1.29×10^{-4}	1555.01	0.6995	0.9530	1.26×10^{-3}	1578.03	0.8966	0.9074	2.51×10^{-3}	1435.96
0.9019	0.9312	1.22×10^{-4}	1479.28	0.7985	0.9364	1.28×10^{-3}	1524.52				
				0.9006	0.9122	2.36×10^{-3}	1443.42				
0.0997	0.9930	2.83×10^{-6}	1605.33	0.0998	0.9905	1.50×10^{-3}	1607.89	0.0909	0.9900	6.43×10^{-4}	1608.81
0.2000	0.9915	5.14×10^{-4}	1702.31	0.1990	0.9909	9.41×10^{-4}	1692.74	0.2002	0.9848	2.16×10^{-4}	1669.73
0.2990	0.9913	1.34×10^{-5}	1714.26	0.2995	0.9847	5.71×10^{-4}	1704.73	0.2996	0.9831	1.12×10^{-3}	1672.36

Table 3 (continued)

[DBA][Ac]						[DBA][Pz]						[DBA][Bu]																	
w_1^d	ρ	$\sigma(\rho)$	ν	$\sigma(\nu)$	w_1^d	ρ	$\sigma(\rho)$	ν	$\sigma(\nu)$	w_1^d	ρ	$\sigma(\rho)$	ν	$\sigma(\nu)$	w_1^d	ρ	$\sigma(\rho)$	ν	$\sigma(\nu)$										
0.5003	0.9794	1.13×10^{-5}	1682.44	0.30	0.4012	0.9795	1.80×10^{-3}	1686.98	0.55	0.4002	0.9745	1.91×10^{-3}	1648.42	0.10	0.5003	0.9794	1.13×10^{-5}	1682.44	0.30	0.4012	0.9795	1.80×10^{-3}	1686.98	0.55	0.4002	0.9745	1.91×10^{-3}	1648.42	0.10
0.5997	0.9701	3.54×10^{-5}	1643.15	0.62	0.4981	0.9731	6.36×10^{-4}	1653.24	0.48	0.5987	0.9525	5.83×10^{-4}	1578.46	0.07	0.5997	0.9701	3.54×10^{-5}	1643.15	0.62	0.4981	0.9731	6.36×10^{-4}	1653.24	0.48	0.5987	0.9525	5.83×10^{-4}	1578.46	0.07
0.7012	0.9594	3.36×10^{-4}	1596.64	0.93	0.6003	0.9626	5.88×10^{-4}	1610.58	0.13	0.6996	0.9361	1.79×10^{-3}	1541.58	0.90	0.7012	0.9594	3.36×10^{-4}	1596.64	0.93	0.6003	0.9626	5.88×10^{-4}	1610.58	0.13	0.6996	0.9361	1.79×10^{-3}	1541.58	0.90
0.8010	0.9445	1.16×10^{-4}	1539.00	0.99	0.6995	0.9491	9.70×10^{-4}	1562.51	0.49	0.8966	0.9037	1.63×10^{-3}	1418.60	1.13	0.8010	0.9445	1.16×10^{-4}	1539.00	0.99	0.6995	0.9491	9.70×10^{-4}	1562.51	0.49	0.8966	0.9037	1.63×10^{-3}	1418.60	1.13
0.9019	0.9274	1.94×10^{-4}	1462.37	1.07	0.7985	0.9323	7.43×10^{-4}	1507.95	1.74	0.9066	0.9068	3.78×10^{-3}	1426.48	0.00	0.9019	0.9274	1.94×10^{-4}	1462.37	1.07	0.7985	0.9323	7.43×10^{-4}	1507.95	1.74	0.9066	0.9068	3.78×10^{-3}	1426.48	0.00
$T = 313.15 \pm 0.01$ K																													
0.0997	0.9909	4.24×10^{-6}	1608.33	0.042	0.0998	0.9877	1.24×10^{-3}	1610.60	0.04	0.0909	0.9870	3.72×10^{-4}	1611.11	0.01	0.0997	0.9909	4.24×10^{-6}	1608.33	0.042	0.0998	0.9877	1.24×10^{-3}	1610.60	0.04	0.0909	0.9870	3.72×10^{-4}	1611.11	0.01
0.2000	0.9885	5.44×10^{-4}	1694.97	0.021	0.1990	0.9881	9.57×10^{-4}	1685.61	0.01	0.2002	0.9813	5.64×10^{-4}	1664.11	0.01	0.2000	0.9885	5.44×10^{-4}	1694.97	0.021	0.1990	0.9881	9.57×10^{-4}	1685.61	0.01	0.2002	0.9813	5.64×10^{-4}	1664.11	0.01
0.2990	0.9883	1.06×10^{-5}	1704.75	0.014	0.2995	0.9810	2.06×10^{-4}	1694.68	0.18	0.2996	0.9794	1.06×10^{-3}	1662.96	0.01	0.2990	0.9883	1.06×10^{-5}	1704.75	0.014	0.2995	0.9810	2.06×10^{-4}	1694.68	0.18	0.2996	0.9794	1.06×10^{-3}	1662.96	0.01
0.5003	0.9759	1.56×10^{-5}	1669.65	0.212	0.4012	0.9754	1.04×10^{-3}	1675.24	0.39	0.4002	0.9710	2.00×10^{-3}	1637.78	0.01	0.5003	0.9759	1.56×10^{-5}	1669.65	0.212	0.4012	0.9754	1.04×10^{-3}	1675.24	0.39	0.4002	0.9710	2.00×10^{-3}	1637.78	0.01
0.5997	0.9666	3.04×10^{-5}	1629.27	0.552	0.4981	0.9693	3.95×10^{-4}	1640.31	0.45	0.5987	0.9485	5.58×10^{-4}	1564.61	0.04	0.5997	0.9666	3.04×10^{-5}	1629.27	0.552	0.4981	0.9693	3.95×10^{-4}	1640.31	0.45	0.5987	0.9485	5.58×10^{-4}	1564.61	0.04
0.7012	0.9559	2.69×10^{-4}	1581.78	0.870	0.6003	0.9589	9.58×10^{-4}	1596.16	0.21	0.6996	0.9314	1.37×10^{-3}	1526.53	0.71	0.7012	0.9559	2.69×10^{-4}	1581.78	0.870	0.6003	0.9589	9.58×10^{-4}	1596.16	0.21	0.6996	0.9314	1.37×10^{-3}	1526.53	0.71
0.8010	0.9410	8.63×10^{-5}	1522.99	0.912	0.6995	0.9451	5.35×10^{-4}	1546.84	0.35	0.8966	0.9000	8.20×10^{-4}	1401.15	0.85	0.8010	0.9410	8.63×10^{-5}	1522.99	0.912	0.6995	0.9451	5.35×10^{-4}	1546.84	0.35	0.8966	0.9000	8.20×10^{-4}	1401.15	0.85
0.9019	0.9235	3.74×10^{-4}	1445.36	0.785	0.7985	0.9282	3.35×10^{-4}	1491.20	1.41	0.9066	0.9085	1.06×10^{-3}	1405.89	0.51	0.9019	0.9235	3.74×10^{-4}	1445.36	0.785	0.7985	0.9282	3.35×10^{-4}	1491.20	1.41	0.9066	0.9085	1.06×10^{-3}	1405.89	0.51
$T = 318.15 \pm 0.01$ K																													
0.0997	0.9887	1.41×10^{-6}	1610.16	0.02	0.0998	0.9839	7.95×10^{-4}	1612.15	0.04	0.0909	0.9841	3.58×10^{-4}	1612.23	0.01	0.0997	0.9887	1.41×10^{-6}	1610.16	0.02	0.0998	0.9839	7.95×10^{-4}	1612.15	0.04	0.0909	0.9841	3.58×10^{-4}	1612.23	0.01
0.2000	0.9854	4.59×10^{-4}	1687.20	0.02	0.1990	0.9851	8.56×10^{-4}	1678.10	0.01	0.2002	0.9763	4.26×10^{-4}	1657.99	0.00	0.2000	0.9854	4.59×10^{-4}	1687.20	0.02	0.1990	0.9851	8.56×10^{-4}	1678.10	0.01	0.2002	0.9763	4.26×10^{-4}	1657.99	0.00
0.2990	0.9852	2.12×10^{-5}	1694.96	0.01	0.2995	0.9773	5.23×10^{-5}	1684.37	0.12	0.2996	0.9757	9.10×10^{-4}	1653.26	0.02	0.2990	0.9852	2.12×10^{-5}	1694.96	0.01	0.2995	0.9773	5.23×10^{-5}	1684.37	0.12	0.2996	0.9757	9.10×10^{-4}	1653.26	0.02
0.5003	0.9724	1.06×10^{-5}	1656.57	0.10	0.4012	0.9716	5.61×10^{-4}	1663.19	0.23	0.4002	0.9679	1.27×10^{-3}	1626.91	0.03	0.5003	0.9724	1.06×10^{-5}	1656.57	0.10	0.4012	0.9716	5.61×10^{-4}	1663.19	0.23	0.4002	0.9679	1.27×10^{-3}	1626.91	0.03
0.5997	0.9631	2.26×10^{-5}	1615.12	0.49	0.4981	0.9656	1.63×10^{-4}	1627.14	0.40	0.5987	0.9442	4.30×10^{-4}	1550.55	0.01	0.5997	0.9631	2.26×10^{-5}	1615.12	0.49	0.4981	0.9656	1.63×10^{-4}	1627.14	0.40	0.5987	0.9442	4.30×10^{-4}	1550.55	0.01
0.7012	0.9524	1.85×10^{-4}	1566.71	0.81	0.6003	0.9551	1.42×10^{-3}	1581.49	0.21	0.6996	0.9265	9.03×10^{-4}	1511.32	0.46	0.7012	0.9524	1.85×10^{-4}	1566.71	0.81	0.6003	0.9551	1.42×10^{-3}	1581.49	0.21	0.6996	0.9265	9.03×10^{-4}	1511.32	0.46
0.8010	0.9374	4.88×10^{-5}	1506.81	0.86	0.6995	0.9412	3.08×10^{-4}	1530.91	0.20	0.8966	0.8959	3.07×10^{-4}	1383.63	0.53	0.8010	0.9374	4.88×10^{-5}	1506.81	0.86	0.6995	0.9412	3.08×10^{-4}	1530.91	0.20	0.8966	0.8959	3.07×10^{-4}	1383.63	0.53
0.9019	0.9197	3.50×10^{-4}	1428.26	0.47	0.7985	0.9241	1.26×10^{-4}	1474.39	0.86	0.9066	0.9052	1.58×10^{-3}	1388.41	0.78	0.9019	0.9197	3.50×10^{-4}	1428.26	0.47	0.7985	0.9241	1.26×10^{-4}	1474.39	0.86	0.9066	0.9052	1.58×10^{-3}	1388.41	0.78
$T = 323.15 \pm 0.01$ K																													
0.0997	0.9863	1.41×10^{-6}	1610.87	0.01	0.0998	0.9802	8.98×10^{-4}	1612.58	0.03	0.0909	0.9807	3.36×10^{-4}	1612.30	0.01	0.0997	0.9863	1.41×10^{-6}	1610.87	0.01	0.0998	0.9802	8.98×10^{-4}	1612.58	0.03	0.0909	0.9807	3.36×10^{-4}	1612.30	0.01
0.2000	0.9821	9.76×10^{-5}	1679.06	0.01	0.1990	0.9818	7.64×10^{-5}	1670.16	0.03	0.2002	0.9712	6.15×10^{-5}	1651.34	0.01	0.2000	0.9821	9.76×10^{-5}	1679.06	0.01	0.1990	0.9818	7.64×10^{-5}	1670.16	0.03	0.2002	0.9712	6.15×10^{-5}	1651.34	0.01
0.2990	0.9820	5.09×10^{-5}	1684.87	0.00	0.2995	0.9736	2.05×10^{-5}	1673.90	0.06	0.2996	0.9706	2.22×10^{-4}	1643.36	0.03	0.2990	0.9820	5.09×10^{-5}	1684.87	0.00	0.2995	0.9736	2.05×10^{-5}	1673.90	0.06	0.2996	0.9706	2.22×10^{-4}	1643.36	0.03
0.5003	0.9688	9.19×10^{-6}	1643.22	0.02	0.4012	0.9678	5.30×10^{-5}	1650.85	0.05	0.4002	0.9630	3.11×10^{-5}	1615.70	0.00	0.5003	0.9688	9.19×10^{-6}	1643.22	0.02	0.4012	0.9678	5.30×10^{-5}	1650.85	0.05	0.4002	0.9630	3.11×10^{-5}	1615.70	0.00
0.5997	0.9595	1.48×10^{-5}	1600.81	0.49	0.4981	0.9617	7.78×10^{-5}	1613.57	0.37	0.5987	0.9397	1.96×10^{-4}	1536.18	0.01	0.5997	0.9595	1.48×10^{-5}	1600.81	0.49	0.4981	0.9617	7.78×10^{-5}	1613.57	0.37	0.5987	0.9397	1.96×10^{-4}	1536.18	0.01
0.7012	0.9488	1.25×10^{-4}	1551.55	0.76	0.6003	0.9510	2.23×10^{-3}	1566.57	0.23	0.6996	0.9216	3.77×10^{-4}	1495.94	0.09	0.7012	0.9488	1.25×10^{-4}	1551.55	0.76	0.6003	0.9510	2.23×10^{-3}	1566.57	0.23	0.6996	0.9216	3.77×10^{-4}	1495.94	0.09
0.8010	0.9337	1.41×10^{-5}	1490.56	0.82	0.6995	0.9373	8.06×10^{-5}	1514.88	0.08	0.8966	0.8917	5.06×10^{-5}	1366.19	0.14	0.8010	0.9337	1.41×10^{-5}	1490.56	0.82	0.6995	0.9373	8.06×10^{-5}	1514.88	0.08	0.8966	0.8917	5.06×10^{-5}	1366.19	0.14
0.9019	0.9158	1.37×10^{-4}	1410.99	0.21	0.7985	0.9200	9.19×10^{-6}	1457.55	0.22	0.9066	0.9200	9.19×10^{-6}	1457.55	0.22	0.9019	0.9158	1.37×10^{-4}	1410.99	0.21	0.7985	0.9200	9.19×10^{-6}	1457.55	0.22	0.9066	0.9200	9.19×10^{-6}	1457.55	0.22

Table 4 Coefficients from the fitted model and evaluation of the quality of the fit

	[DBA][Ac]		[DBA][Pr]		[DBA][Bu]	
	Density	Speed of sound	Density	Speed of sound	Density	Speed of sound
B ₀₀	6.37×10^{-1}	3.31×10^3	3.36	2.37×10^3	4.99×10^{-1}	3.00×10^3
B ₀₁	2.55×10^{-3}	- 7.89	$- 1.54 \times 10^{-2}$	- 1.84	3.19×10^{-3}	- 6.34
B ₀₂	$- 5.40 \times 10^{-6}$	5.69×10^{-3}	2.38×10^{-5}	$- 4.41 \times 10^{-3}$	$- 6.31 \times 10^{-6}$	3.40×10^{-3}
B ₁₀	$- 1.75 \times 10^{-1}$	$- 1.24 \times 10^4$	- 6.66	$- 6.03 \times 10^3$	1.76	$- 6.45 \times 10^3$
B ₁₁	2.27×10^{-3}	7.19×10^1	4.52×10^{-2}	3.09×10^1	$- 9.09 \times 10^{-3}$	3.57×10^3
B ₁₂	$- 3.42 \times 10^{-6}$	$- 9.79 \times 10^{-2}$	$- 7.41 \times 10^{-5}$	$- 3.21 \times 10^{-2}$	1.33×10^{-5}	$- 4.34 \times 10^{-2}$
B ₂₀	1.30	3.59×10^4	3.67	2.19×10^4	$- 2.08 \times 10^{00}$	1.42×10^4
B ₂₁	$- 9.49 \times 10^{-3}$	$- 1.99 \times 10^2$	$- 2.54 \times 10^{-2}$	$- 1.11 \times 10^2$	1.16×10^{-2}	$- 6.79 \times 10^1$
B ₂₂	1.58×10^{-5}	2.77×10^{-1}	4.23×10^{-5}	1.38×10^{-1}	$- 1.68 \times 10^{-5}$	7.77×10^{-2}
B ₃₀		$- 3.01 \times 10^4$		$- 2.08 \times 10^4$		$- 1.08 \times 10^4$
B ₃₁		1.63×10^2		1.06×10^2		4.67×10^1
B ₃₂		$- 2.25 \times 10^{-1}$		$- 1.36 \times 10^{-1}$		$- 4.75 \times 10^{-2}$
%AARD	7.49×10^{-2}	5.00×10^{-1}	1.23×10^{-1}	7.00×10^{-1}	1.25×10^{-1}	4.00×10^{-1}
R ²	9.98×10^{-1}	9.88×10^{-1}	9.97×10^{-1}	9.89×10^{-1}	9.97×10^{-1}	9.91×10^{-1}

**Fig. 1** **a** [DBA][Ac] density and **b** speed of sound data as a function of ionic liquid mass fraction. Black: 293.15 K; red: 298.15 K; green: 303.15 K; blue: 308.15 K; cyan: 313.15 K; magenta: 318.15 K; yellow: 323.15 K

(Fig. 4a), and as shown in Figs. S6(a) and S7(a) in the Supplementary Material.

To gather electrochemical data, solutions with concentrations of ~0.1 to ~0.9 g/g were used. Fig. S8 in the Supplementary Material presents the Nyquist diagrams for the [DBA][Ac], [DBA][Pr], and [DBA][Bu] solutions.

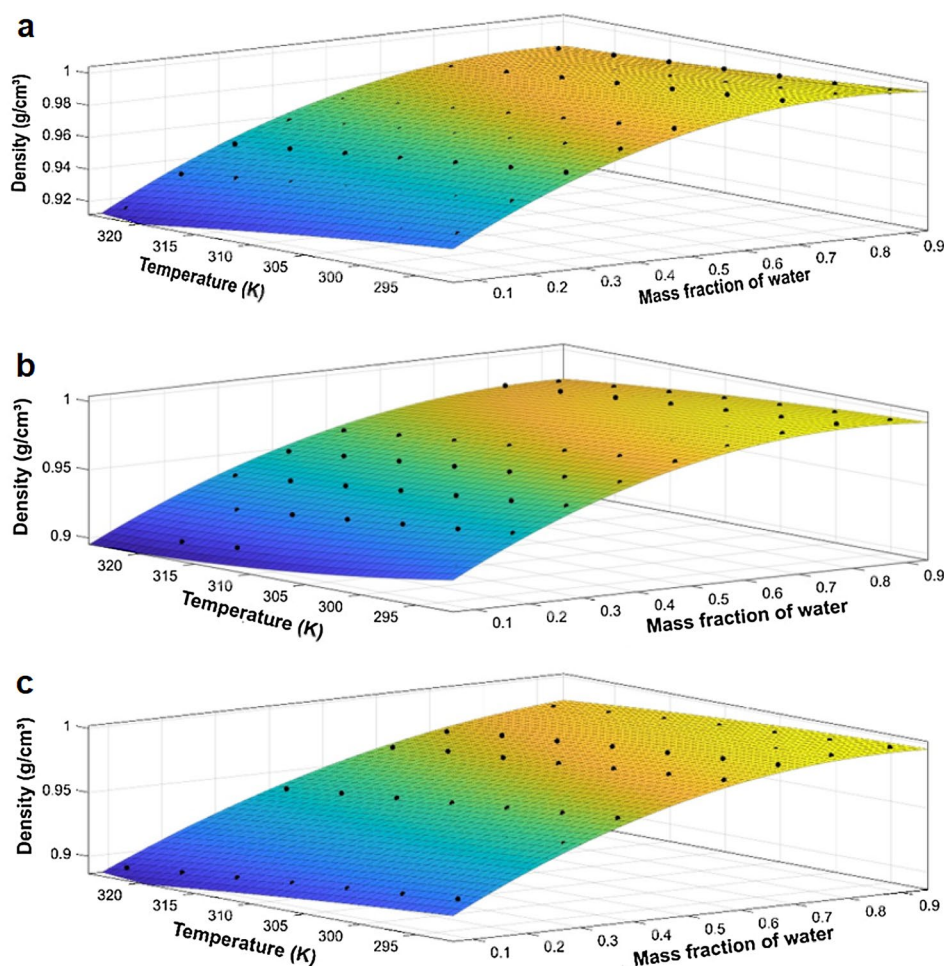
For the three analyzed ILs, the behavior of the solutions was very similar. When the slopes of the lines formed by the points of equal concentrations of IL exceed an angle of 45°, the solutions exhibit a behavior with more capacitive than resistive characteristics. With an increase in the concentration of IL in the solution, the points shift to values indicating greater real resistance. The resistance tends to increase as the

concentration of IL increases, whereas an inversion occurs at low concentrations. That is, the ionic liquid is more conductive in a more dilute solution. In addition, when comparing the resistance values of the three analyzed ILs, it appears that the resistance tends to increase with an increase in the length of the carbon chain.

The electrical conductivity data were extracted from the Nyquist diagrams, and the results are presented in Table 5.

From the data in Table 5, it is observed that in solutions between ~0.1 and ~0.4 g/g of IL, the increasing resistance trend with increasing IL concentration is not observed. This effect occurs owing to the formation of micelles in the system, which influences the resistance of the medium because

Fig. 2 Density as a function of temperature and mass fraction of water for **a** [DBA][Ac], **b** [DBA][Pr], and **c** [DBA][Bu] mixtures. The dots represent the experimental data, and the surface was fitted to these data



the micelle bodies inhibit the conductivity and electrical resistance, as these properties depend on the constituents in the medium.

Even if the mass concentration is maintained, there may be variations in the concentrations of charge-carrying particles in the system because a micelle is a cluster of particles. Therefore, for example, two solutions consisting of two different types of ILs with the same mass concentration can present different resistance results because one IL in the solution can form micelles in greater quantity, which reduce the number of free particles available for charge transport. As previously mentioned, this occurs because the ability to form micelles is related to the size of the carbon chain. In this case, solutions containing larger carbon chains are more prone to micellar formation.

Figure 5 shows the conductivity as a function of the IL mass fraction, and more clearly indicates how the formation of micelles affects the system.

Above a certain concentration, surfactants spontaneously begin to form micelles. This concentration defines the critical micellar concentration (CMC) point (Hezave et al. 2013). The coordinate points where the lines intersect indicate the

approximate concentrations at which the CMC is reached. This reiterates the surfactant properties of the studied ILs. Additional data are presented in Table 6.

The IL solutions that presented the highest conductivities were [DBA][Ac] and [DBA][Pr] because their smaller ions can move more easily than the larger ions in [DBA][Bu]. From the data in Table 6, it can be seen that as the carbonic anion chain of the ILs increases, lower concentrations are needed to reach the CMC point. As a consequence, the values of the impedance of the solutions, as well as the density and speed of sound, decrease.

Nascimento et al. (2020) analyzed the conductivity of diethylammonium acetate [DEA][Ac] and obtained conductivity ranging from 0.0155 to 0.0036 S/cm. In this work, the conductivities obtained from all ILs ranged from 0.0134 to 0.0007 S/cm. For the same temperature, pressure, and similar molar fraction range, both works showed conductivities in the same range. The conductivities of [DEA][Ac] were slightly higher, this can be attributed to the smaller size of the cation (DEA) and anion (in comparison with propionate and butanoate (also studied in this work), which facilitates mobility leading to higher conductivity.

Fig. 3 Speed of sound as a function of temperature and mass fraction of water for **a** [DBA][Ac], **b** [DBA][Pr], and **c** [DBA][Pr] mixtures. The dots represent the experimental data, and the surface was fitted to these data

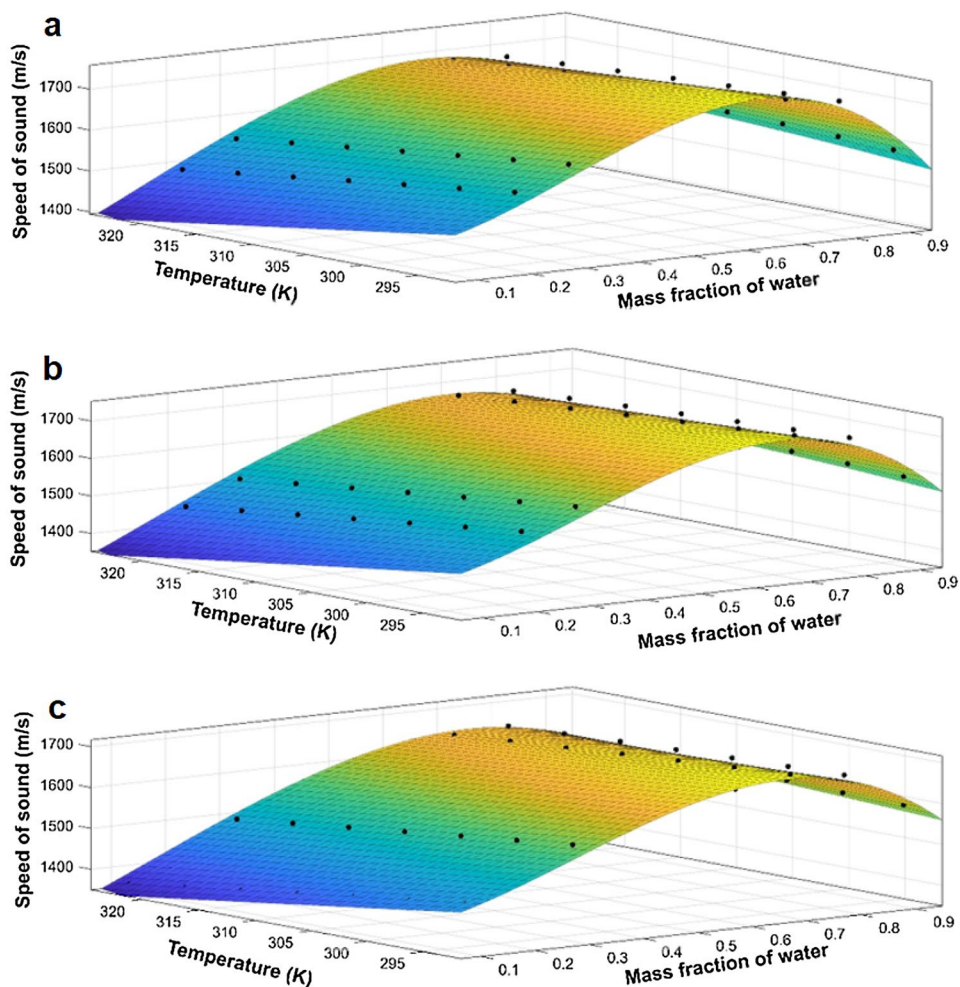


Table 5 Data obtained from the Nyquist diagrams for [DBA][Ac], [DBA][Pr], and [DBA][Bu], where w_1 is the IL mass fraction, K is the conductivity measured at an average temperature and uncertainty of 298 ± 1 K, and $u(K)$ is the conductivity uncertainty (atmospheric pressure of 101.39 ± 0.21 kPa)

[DBA][Ac]			[DBA][Pr]			[DBA][Bu]		
w_1^a	K	$u(K)$	w_1^a	K	$u(K)$	w_1^a	K	$u(K)$
(g/g)	(S/cm)	(S/cm)	(g/g)	(S/cm)	(S/cm)	(g/g)	(S/cm)	(S/cm)
0.0997	0.0134	1.71×10^{-4}	0.0998	0.0104	1.04×10^{-4}	0.0909	0.0110	1.16×10^{-4}
0.1999	0.0163	2.57×10^{-4}	0.1997	0.0162	2.52×10^{-4}	0.2002	0.0133	1.69×10^{-4}
0.2998	0.0161	2.50×10^{-4}	0.2995	0.0160	2.45×10^{-4}	0.2996	0.0127	1.55×10^{-4}
0.4007	0.0142	1.95×10^{-4}	0.4012	0.0132	1.67×10^{-4}	0.4002	0.0107	1.11×10^{-4}
0.5003	0.0118	1.33×10^{-4}	0.4981	0.0107	1.10×10^{-4}	0.4991	0.0086	7.17×10^{-5}
0.5997	0.0084	6.83×10^{-5}	0.6003	0.0078	5.78×10^{-5}	0.5987	0.0065	4.06×10^{-5}
0.7012	0.0050	2.43×10^{-5}	0.6995	0.0051	2.47×10^{-5}	0.6996	0.0046	2.07×10^{-5}
0.8006	0.0025	5.85×10^{-6}	0.7985	0.0025	6.17×10^{-6}	0.7964	0.0022	4.63×10^{-6}
0.9019	0.0008	6.42×10^{-7}	0.9006	0.0009	7.51×10^{-7}	0.8966	0.0007	5.40×10^{-7}

^a $U(w_1^a) \pm 0.0005$ g/g

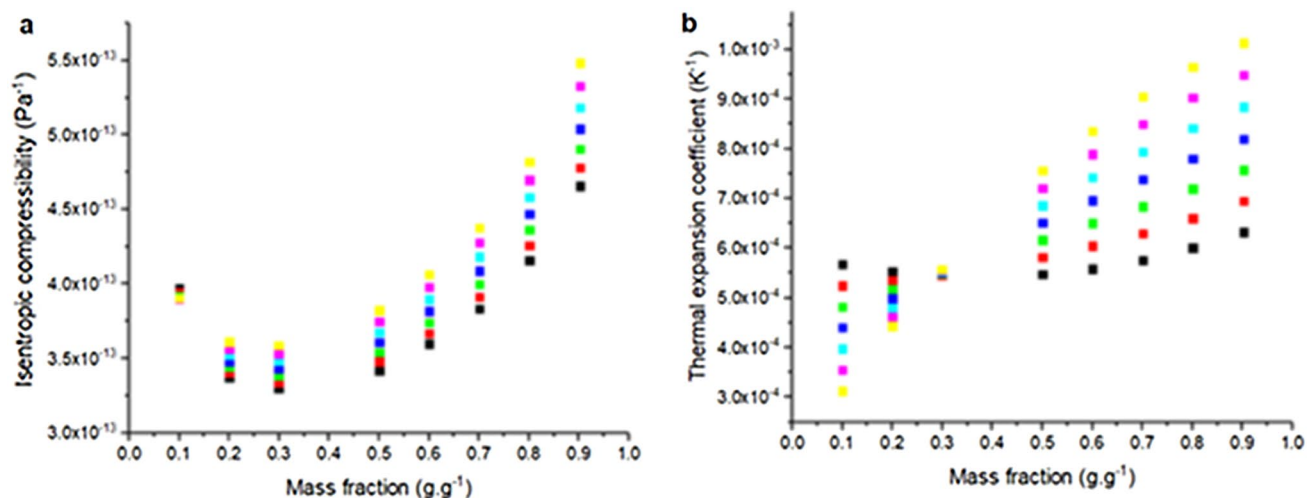


Fig. 4 Isotherms of **a** isentropic compressibility and **b** thermal expansion coefficient as a function of IL mass fraction for [DBA][Ac]. Black: 293.15 K; red: 298.15 K; green: 303.15 K; blue: 308.15 K; cyan: 313.15 K; magenta: 318.15 K; yellow: 323.15 K

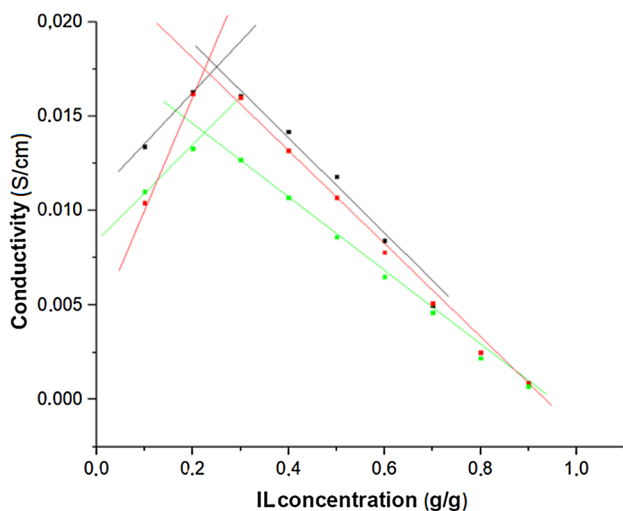


Fig. 5 Conductivity of ionic liquids by mass fraction of IL in g/g measured at 298 298 ± 1 K and 101.39 ± 0.21 kPa. The intersections of lines of the same color indicate conductivity inflection points in the solutions. Black: [DBA][Ac]; red: [DBA][Pr]; green: [DBA][Bu]

Table 6 IL conductivity data in the vicinity of the CMC. Concentration and conductivity were measured at an average temperature of 298 ± 1 K, and $u_{(K)}$ is the conductivity uncertainty (atmospheric pressure of 101.39 ± 0.21 kPa)

IL	Conductivity (K) at CMC S/cm	U(K) S/cm	CMC ^a g/g
[DBA][Ac]	0.0163	2.54×10^{-4}	0.254
[DBA][Pr]	0.0156	2.48×10^{-4}	0.279
[DBA][Bu]	0.0128	1.62×10^{-4}	0.234

^aU(CMC) ± 0.001 g

Conclusions

Three ionic liquids were synthesized for this study based on the Brønsted-Lowry acid-neutralization reaction: dibutylammonium acetate, dibutylammonium propanoate, and dibutylammonium butanoate. Density, speed of sound, and conductivity measurements were performed at temperatures from 293.15 to 323.15 K under atmospheric pressure. The derived properties were calculated using the obtained experimental data, namely, the thermal expansion coefficient and isentropic compressibility.

The results indicate that an increase in the length of the anion carbon chain from 2 to 4 carbons has a tendency to decrease the density and speed of sound for concentrations ranging from 0.4 to 0.9 g/g. However, in the range of 0.2–0.3 g/g, this pattern was not observed owing to micelle formation. The CMC points for the three ILs were between 0.23 g/g and 0.28 g/g at 298 K. Measured conductivity values varied between 0.0004 S/cm and 0.0163 S/cm at 298 K.

The calculated isentropic compressibility showed that all three ILs exhibited similar behavior and had a minimum in the CMC range. In other words, the shorter the anion chain length is, the lower the isentropic compressibility value, following the order: [DBA][Ac] < [DBA][Pr] < [DBA][Bu]. For the thermal expansion coefficient, it was shown that for most solutions, increasing the concentration of IL in the solution increasingly affects the coefficient.

From the presented data, it can be concluded that the most significant changes occurred in the water-rich regions. The thermodynamic data obtained in this study can contribute to the development of a database that provides the

physical–chemical properties of binary aqueous solutions of protic ionic liquids. In addition, understanding the behavior and deviations of these binary solutions, such as volumetric and sound properties, helps to understand the behavior of protic ionic fluids under various conditions.

Supplementary Information The online version contains supplementary material available at <https://doi.org/10.1007/s43153-021-00174-7>.

Acknowledgements This study was funded by Fundação de Amparo à Pesquisa (FAPESP/SECTI/Bahia/Brazil, Project APP075/2016 and Grants BOL0426/2018, BOL2322/2019); Conselho Nacional de Desenvolvimento Científico e Tecnológico (CNPq/Brazil, Project 438036/2018-2 and Grant 303089/2019-9) and Coordenação de Aperfeiçoamento de Pessoal de Nível Superior—Brazil (CAPES).

Declarations

Conflict of interest The authors declare that they have no competing financial interests or personal relationships that could have influenced the study reported in this paper.

References

- Alcantara ML, Santos JP, Loreno M, Ferreira PI, Paredes ML, Caradozo-Filho L, Mattedi S (2018) Low viscosity protic ionic liquid for CO₂/CH₄ separation: thermophysical and high-pressure phase equilibria for diethylammonium butanoate. *Fluid Phase Equilib* 459:30–43
- Alvarez VH, Mattedi S, Martin-Pastor M, Aznar M, Iglesias M (2011) Thermophysical properties of binary mixtures of {ionic liquid 2-hydroxy ethylammonium acetate + (water, methanol, or ethanol)}. *J Chem Thermodyn* 43(7):997–1010
- Alvarez VH, Mattedi S, Aznar M (2013) Density, refraction index and vapor–liquid equilibria of *N*-methyl-2-hydroxyethylammonium butyrate plus (methyl acetate or ethyl acetate or propyl acetate) at several temperatures. *J Chem Thermodyn* 62:130–141
- Armand M, Endres F, MacFarlane DR, Ohno H, Scrosati B (2009) Ionic-liquid materials for the electrochemical challenges of the future. *Nat Mater* 8:621–629
- Balducci A, Jeong SS, Kim GT, Passerini S, Winter M, Schmuck M, Tran N (2011) Development of safe, green and high performance ionic liquids-based batteries (ILLIBATT project). *J Power Sour* 196:9719–9730
- Basouli H, Mozaffari F, Eslami H (2021) Atomistic insights into structure, ion-pairing and ionic conductivity of 1-ethyl-3-methylimidazolium methylsulfate [Emim][MeSO₄] ionic liquid from molecular dynamics simulation. *J Mol Liq* 331:115803
- Bittencourt SS, Hoga HE, Torres RB, d'Angelo JV (2017) Thermodynamic and spectroscopic properties of binary mixtures of *n*-butylammonium butanoate ionic liquid with alcohols at $T = (293.15–313.15)$ K. *J Chem Thermodyn* 105:238–252
- Borgel V, Markevich E, Aurbach D, Semrau G, Schmidt M (2009) On the application of ionic liquids for rechargeable Li batteries: high voltage systems. *J Power Sour* 189:331–336
- Buzzeo MC, Evans RG, Compton RG (2004) Non-haloaluminate room-temperature ionic liquids in electrochemistry—a review. *ChemPhysChem* 5:1106–1120
- Cervera TG, Vega-Leal AP, García GA, Sánchez JB (2014) PEMFC impedance spectroscopy using synthetic wide-band signals. *Int J Hydrogen Energy* 39(8):4005–4008
- Crespo EA, Silva LP, Correia CIP, Martins MAR, Gardas RL, Vega LF, Carvalho PJ, Coutinho JAP (2021) Development of a robust soft-SAFT model for protic ionic liquids using new high-pressure density data. *Fluid Phase Equilib* 539:113036
- Darabi R, Shabani-Nooshabadi M (2021) NiFe₂O₄-rGO/ionic liquid modified carbon paste electrode: an amplified electrochemical sensitive sensor for determination of sunset yellow in the presence of Tartrazine and Allura Red. *Food Chem* 339:127841
- Eftekhari A, Liu Y, Chen P (2016) Different roles of ionic liquids in lithium batteries. *J Power Sour* 334:221–239
- Greaves TL, Ha K, Muir BW, Howard SC, Weerawardena A, Kirby N, Drummond CJ (2015) Protic ionic liquids (PILs) nanostructure and physicochemical properties: development of high-throughput methodology for PIL creation and property screens. *Phys Chem Chem Phys* 17(4):2357–2365
- Hezave AZ, Dorostkar S, Ayatollahi S, Nabipour M, Hemmateenejad B (2013) Effect of different families (imidazolium and pyridinium) of ionic liquids-based surfactants on interfacial tension of water/crude oil system. *Fluid Phase Equilib* 360:139–145
- Kar M, Winther-Jensen B, Forsyth M, MacFarlane DR (2013) Chelating ionic liquids for reversible zinc electrochemistry. *Phys Chem Chem Phys* 15:7191–7197
- Khan A, Gusain R, Khatri OP (2018) Organophosphate anion based low viscosity ionic liquids as oil-miscible additives for lubrication enhancement. *J Mol Liq* 272:430–438
- Keshapolla D, Srinivasarao K, Gardas RL (2019) Influence of temperature and alkyl chain length on physicochemical properties of trihexyl- and trioctylammonium based protic ionic liquids. *J Chem Thermodyn* 133:170–180
- Kong Z, Li L, Xue Y, Yang M, Li Y-Y (2019) Challenges and prospects for the anaerobic treatment of chemical-industrial organic wastewater: a review. *J Clean Prod* 231:913–927
- Li J, Wang S, Liu F, Wang X, Chen H, Mao T, Wang Z (2019) Poly (aryl ether ketone)/polymeric ionic liquid with anisotropic swelling behavior for anion exchange membranes. *J Membr Sci* 581:303–311
- Lu W, Fadeev GA, Qi B, Smela E, Mattes BR, Forsyth M (2002) Use of ionic liquids for π -conjugated polymer electrochemical devices. *Science* 297:983–987
- MacFarlane DR, Seddon KR (2007) Ionic liquids—progress on the fundamental issues. *Aust J Chem* 60(1):3–5
- Malik S, Gupta H, Sharma VK (2021) Molecular interactions in ternary liquid mixtures containing alkyl imidazolium tetrafluoroborates and cyclic ketones: Excess molar volumes and excess isentropic compressibilities. *Chem Data Collect* 31:100603
- Maximo GJ, Santos RJB, Lopes-da-Silva JA, Costa MC, Meirelles AJA, Coutinho JAP (2014) Lipidic protic ionic liquid crystals. *ACS Sustain. Chem Eng* 2(4):672–682
- Mert S, Bankoğlu B, Özkan A, Atar N, Yola ML (2018) Electrochemical sensing of ractopamine by carbon nitride nanotubes/ionic liquid nanohybrid in presence of other β -agonists. *J Mol Liq* 254:8–11
- Musale SP, Patil KR, Gavhane RJ, Dagade DH (2018) Density and speed-of-sound measurements for dilute binary mixtures of diethylammonium-based protic ionic liquids with water. *J Chem Eng Data* 63(6):1859–1876
- Nair MG, Mohapatra SR (2019) Perchloric acid functionalized nanosilica and protic ionic liquid based non-aqueous proton conductive polymer electrolytes. *Mater Lett* 251:148–151
- Nascimento AD, dos Reis R, Santos JPS, Mattedi S, Senna LF (2020) Thermophysical properties of diethylammonium (acetate+water) mixtures at different temperatures. *J Chem Thermodyn* 145:106093
- Oliveira MVS, Vidal BT, Melo CM, Miranda RCM, Soares CMF, Coutinho JAP, Mattedi S, Lima AS (2016) (Eco) toxicity and biodegradability of protic ionic liquids. *Chemosphere* 147:460–466

- Pinkert A, Ang KL, Marsh KN, Pang S (2011) Density, viscosity and electrical conductivity of protic alkanolammonium ionic liquids. *Phys Chem Chem Phys* 13(11):5136–5143
- Rosales G, Alves F, Costa F, Martín Pastor M, Fernandes VC, Mattedi S, Boaventura JS (2019) Development of a bioelectrode based on catalase enzyme and the novel protic ionic liquid pentaethylenehexammonium acetate (PEHAA). *J Mol Liq* 280:182–190
- Sakaabe H, Matsumoto H (2003) *N*-methyl-*N*-propylpiperidinium bis(trifluoromethanesulfonyl)imide (PP13-TFSI)—novel electrolyte base for Li battery. *Electrochem Commun* 5:594–598
- Sarabando JA, Magano PJM, Ferreira AGM, Santos B, Carvalho PJ, Mattedi S, Fonseca IMA, Santos M (2019) Influence of temperature and pressure on the density and speed of sound of *N*-ethyl-2-hydroxyethylammonium propionate ionic liquid. *J Chem Thermodyn* 131:303–313
- Santos MO, Santos GOS, Mattedi S, Griza S, Eguiluz KIB, Salazar-Banda GR (2018) Influence of the calcination temperature and ionic liquid used during synthesis procedure on the physical and electrochemical properties of Ti/(RuO₂) 0.8–(Sb₂O₄) 0.2 anodes. *J Electroanal Chem* 829:116–128
- Shekaari H, Mansoori Y, Sadeghi R (2008) Density, speed of sound, and electrical conductance of ionic liquid 1-hexyl-3-methylimidazolium bromide in water at different temperatures. *J Chem Thermodyn* 40(5):852–859
- Shekaari H, Golmohammadi B, Faraji S, Mokhtarpour M, Sadrmousavi A, Fattah SG, Zafarani-Moattar MT (2021) Thermodynamic and computational study of paracetamol in aqueous solutions of some sustainable amino acid-based ionic liquids. *J Chem Thermodyn* 155:106348
- Shiddiky MJ, Torriero AA (2011) Application of ionic liquids in electrochemical sensing systems. *Biosens Bioelectron* 26:1775–1787
- Song Z, Yan Q, Xia M, Qi X, Zhang Z, Wei J, Fang D, Ma X (2021) Physicochemical properties of *N*-alkylpyridine trifluoroacetate ionic liquids [C_nPy][TFA](*n*= 2–6). *J Chem Thermodyn* 155:106366
- Xu Y, Yao J, Wang C, Li H (2012) Density, viscosity, and refractive index properties for the binary mixtures of *n*-butylammonium acetate ionic liquid + alkanols at several temperatures. *J Chem Eng Data* 57(2):298–308
- Yalsin D, Drummond CJ, Greaves TL (2020) Solvation properties of protic ionic liquids and molecular solvents. *Phys Chem Chem Phys* 22:114–128
- Yoshizawa M, Xu W, Angell CA (2003) Ionic liquids by proton transfer: vapor pressure, conductivity, and the relevance of ΔpK_a from aqueous solutions. *J Am Chem Soc* 125(50):15411–15419
- Zailani NHZO, Yunus NM, Ab Rahim AH, Bustam MA (2020) Thermophysical properties of newly synthesized ammonium-based protic ionic liquids: effect of temperature, anion and alkyl chain length. *Processes* 8(6):742

Publisher's Note Springer Nature remains neutral with regard to jurisdictional claims in published maps and institutional affiliations.